ELSEVIER

Tectonophysics 348 (2002) 73–92

TECTONOPHYSICS

www.elsevier.com/locate/tecto

Fluid flow, alteration and polysulphide mineralisation associated with a low-angle reverse shear zone in the Lower Palaeozoic of the Anglo-Brabant fold belt, Belgium

K. Piessens [a], Ph. Muchez [a,*], S. Dewaele [a], A. Boyce [b], W. De Vos [c], M. Sintubin [d], T.N. Debacker [e], E.A.J. Burke [f], W. Viaene [a]

[a] *Fysico-chemische Geologie, K.U. Leuven, Celestijnenlaan 200C, B-3001 Leuven, Belgium*
[b] *Isotope Geosciences Unit, SURRC, Rankine Avenue, East Kilbride, Glasgow G75 0QF, UK*
[c] *Geological Survey of Belgium, Jennerstraat 13, B-1000 Brussel, Belgium*
[d] *Structurele Geologie en Tektoniek, K.U. Leuven, Redingenstraat 16, B-3000 Leuven, Belgium*
[e] *Vakgroep Geologie en Bodemkunde, Universiteit Gent, Krijgslaan 281 S8, B-9000 Gent, Belgium*
[f] *Faculty of Earth Sciences, Vrije Universiteit, De Boelelaan 1085, NL-1081 HV Amsterdam, The Netherlands*

Received 11 November 2000; accepted 12 June 2001

Abstract

In the Lower Palaeozoic rocks of the Brabant Massif (Belgium), a recently discovered polysulphide mineralisation is related to a low-angle reverse shear zone. This shear zone has been attributed to the main early Devonian deformation event. Data from boreholes and outcrops allow a detailed investigation of the alteration pattern and palaeofluid flow along this shear zone. Macroscopic observations of the mineralogy and quantitative changes in the phyllosilicate mineralogy indicate that this shear zone is characterised by an envelope of intense sericitisation and silicification. In addition, chloritisation is associated with this alteration. The alteration zone may reach a thickness of 250 m. Ore mineralisation occurred synkinematically and is spatially related to the shear zone. The mineralisation consists of pyrite, marcasite, arsenopyrite, pyrrhotite, chalcopyrite, sphalerite, galena, stibnite and smaller amounts of tetrahedrite and other sulphosalts. It is concentrated in quartz–sulphide veins or occurs diffusely in the host rock. The mineralising fluids have a low-salinity $H_2O–CO_2–CH_4–NaCl–(KCl)$ composition and a minimum temperature of 250–320 °C. The $\delta^{18}O$ values of quartz vary between +12.3‰ and +14.5‰ SMOW, and δD compositions of the fluid inclusions in the quartz crystals range from −65‰ to −35‰ V-SMOW. The δD and the calculated $\delta^{18}O$ values of the mineralising fluids fall in the range typical for metamorphic fluids and partly overlap with that for primary magmatic fluids. The $\delta^{34}S$ values, between +4.7‰ and +10.6‰ CDT, fall outside the interval typical for I-type magmas. Important migration of likely metamorphic fluids, causing a widespread alteration and a polysulphide mineralisation along a low-angle shear zone, has, thus, been identified for the first time in the Caledonian Anglo-Brabant fold belt.

Keywords: Brabant Massif; Fluid inclusions; Low-angle shear zone; Lower Palaeozoic; Polysulphide mineralisation; Sericitisation; Stable isotopes

* Corresponding author. Tel.: +32-16-327-584; fax: +32-16-327-981.
E-mail address: philippe.muchez@geo.kuleuven.ac.be (Ph. Muchez).

0040-1951/02/$ - see front matter
PII: S0040-1951(01)00250-5

1. Introduction

Fluid flow in the deeper subsurface is often largely influenced by faults, which can act as highly permeable pathways. In an extensional tectonic regime, substantial quantities of fluids are expelled during normal faulting (Muir-Wood and King, 1993). Fluid migration is often dominated by the convective circulation of chemically evolved meteoric water (Nesbitt and Muehlenbachs, 1989; Kyser and Kerrich, 1990; Travé et al., 1998). In a region of compressional deformation, arrays of subhorizontal extension fractures develop by hydraulic fracturing adjacent to reverse faults prior to failure (Sibson, 1994). These fractures form a substantial lithostatically pressured fluid reservoir. Failure of the reverse faults allows fluids from the overpressured reservoirs to migrate upwards. Typical examples of such a fault-valve action are the mesothermal gold–quartz lodes hosted in steep reverse faults and brittle–ductile shear zones (Sibson et al., 1988; Cox et al., 1991; Robert et al., 1995). The major mesothermal deposits occur in Archaean greenstone sequences (Kerrich, 1987; Roberts, 1987), but important gold production has also come from Palaeozoic (Murphy and Roberts, 1997; Mason, 1997; Bottrell et al., 1988), Mesozoic (Sibson et al., 1988) and Cenozoic (Pettke et al., 1999) vein systems. Polysulphide mineralisation is often associated with the gold-bearing fluids (Touray et al., 1989; Duller et al., 1997; Ixer et al., 1997), but these do not reach economic grades.

These mineralisations are widespread and mostly situated along deep-seated, high-angle shear zones. Although low-angle shear zones are also quite common, mineralisations associated with these zones seem to be rare. Examples of these are the gold-bearing Hyde–Macreas Shear Zone in New Zealand (Teagle et al., 1990; Craw et al., 1999) and the Revenge gold mine in West Australia (Nguyen et al., 1998).

Both in the Archaean (Huizenga, 1995) and in the Phanerozoic (Murphy and Roberts, 1997), lode gold deposits are not only spatially associated with reverse faults or shear zones but also with granitic intrusions. The origin of the mineralising fluids has often been a matter of debate (cf. Groves, 1993). Only a multidisciplinary study, including structural, petrographic, mineralogical and geochemical analyses, allows to determine the origin of the mineralising fluids.

The southwestern margin of the predominantly concealed, Lower Palaeozoic Brabant Massif, just northeast of the Caledonian deformation front (Sintubin, 1999), is characterised by a complex and particular deformation history. This is primarily due to the inferred presence of a rigid granitoid basement block at depth (Everaerts et al., 1996; Sintubin, 1999). South vergent overthrusting on top of this basement block has been demonstrated. The low-angle reverse shear zone, identified in the Marcq area (Debacker, 1999), is an example of this particular tectonic setting.

The aim of this study is to demonstrate that important fluid migration accompanied shear zone development and is responsible for synkinematic alteration and mineralisation. The area has been selected for a detailed investigation since geochemical and geophysical prospection indicated that the WNW–ESE trending area, parallel to the structural grain of the southwestern Brabant Massif, shows disperse but persistent occurrences of sulphides in boreholes. It was considered to have the largest metallogenic potential. The area furthermore allows specifying the processes active along a polysulphide mineralised low-angle shear zone, which is to our knowledge, unique within the Anglo-Brabant fold belt. The regional significance of this observation with respect to the Caledonian deformation history of the Anglo-Brabant fold belt will be discussed.

2. Geological setting

The Lower Palaeozoic Brabant Massif in Belgium forms the southeastern extremity of the Anglo-Brabant fold belt (Pharaoh et al., 1995), itself forming the eastern branch of the British–Belgian Caledonides. This Caledonian slate belt is moulded around the Cadomian Midlands Microcraton, forming the core of the East Avalonia microcontinent (Blundell et al., 1992).

The overall architecture of the Brabant Massif (Fig. 1) consists of a predominantly Cambrian core bordered by Ordovician–Silurian foreland basins (Van Grootel et al., 1997). Based on aeromagnetic data (Chacksfield et al., 1993), a major, high-angle tectonic break is considered to limit the Cambrian core to the south. This break is currently interpreted as a major dextral transpressional shear zone, the Asquempont Shear Zone (ASZ) (Sintubin et al., 1998; Sintubin,

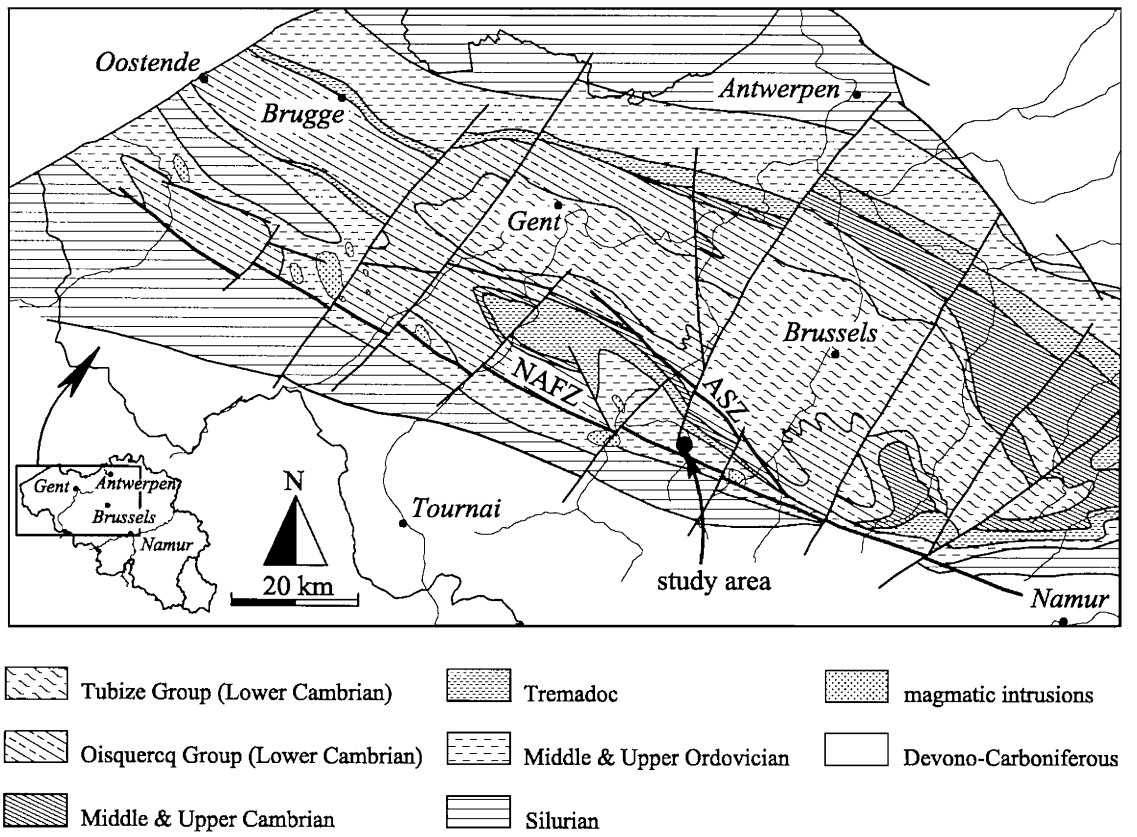

Fig. 1. Subcrop map of the Brabant Massif (after De Vos et al., 1993), with indication of the study area. NAFZ: Nieuwpoort–Asquempont Fault Zone; ASZ: Asquempont Shear Zone.

1999), which largely coincides with the trace of the Asquempont Fault as defined by Legrand (1967) in outcrop. A late Ordovician magmatic arc has been postulated between the Cambrian core and the Ordovician–Silurian foreland basin (Van Grootel et al., 1997). Based on gravimetric data (Everaerts et al., 1996), a granitoid body is inferred at depth. It has been interpreted as a granitic batholith underlying the magmatic arc (Mansy et al., 1999) or as a granitoid basement block of Cadomian age (Sintubin, 1999). To the southwest of the Cambrian core, a NW–SE trending fault zone, the Nieuwpoort–Asquempont Fault Zone, is also apparent on the aeromagnetic map (Chacksfield et al., 1993). This fault zone is still seismically active, as proven by the 1938 Oudenaarde earthquake. However, its origin is unknown (Mansy et al., 1999). The geological subcrop maps of the Brabant Massif (Legrand, 1967; De Vos et al., 1993) furthermore show some NE–SW trending transverse faults segmenting the entire Lower Palaeozoic basement.

One major tectonometamorphic event has been identified, affecting the whole Cambrian to Silurian sedimentary pile (Van Grootel et al., 1997; Debacker et al., 1999). Metamorphism ranges from diagenetic to greenschist. Its spatial distribution suggests a structural and stratigraphical control. Due to the limited degree of exposure, regional fold structures can only be based on the spatial distribution of the distinct lithostratigraphical domains, as expressed on the subcrop map (De Vos et al., 1993), and on the interpretation of the aeromagnetic lineaments (Sintubin, 1997, 1999; Sintubin et al., 1998). Secondary fold structures, which are occasionally observed in the field, suggest an overall SW to S vergence along the south-

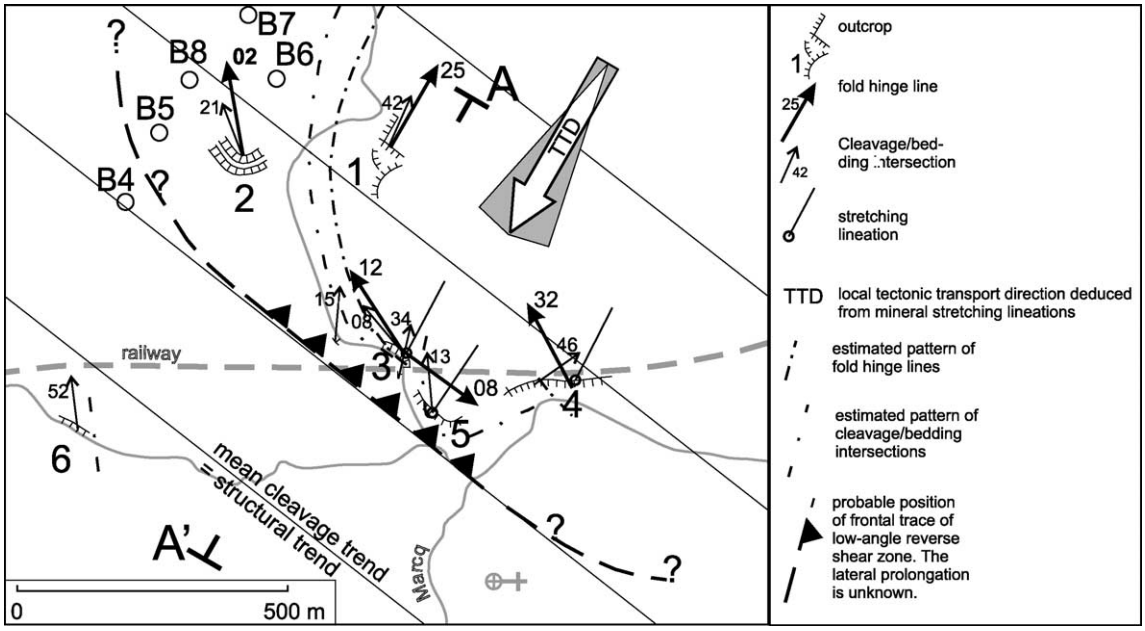

Fig. 2. Compilation of the structural data of the Marcq area with the orientation of the fold hinge lines, the cleavage/bedding intersections and the stretching lineations. Also shown are the mean trend of the NE-dipping cleavage, the deduced position of the low-angle shear zone and patterns of the fold hinge lines (after Debacker, 1999). Numbers refer to the outcrops and B4–B8 to the location of the boreholes studied. The profile A–A′ is given in Fig. 3.

western and southern margin of the Brabant Massif. Broadly coeval with the main folding event, a pervasive cleavage developed.

The Lower Palaeozoic basement is unconformably overlain by Givetian deposits, lacking any regional cleavage development or metamorphism. Metamorphism, folding and cleavage development in the Brabant Massif, thus, predates the Givetian and postdates the Gorstian, the youngest sediments affected. The tectonometamorphic event affecting the Lower Palaeozoic of the Brabant Massif most probably took place during the early Devonian (André et al., 1981; Verniers and Van Grootel, 1991). This event can be ascribed to a post-accretionary intracontinental accom-

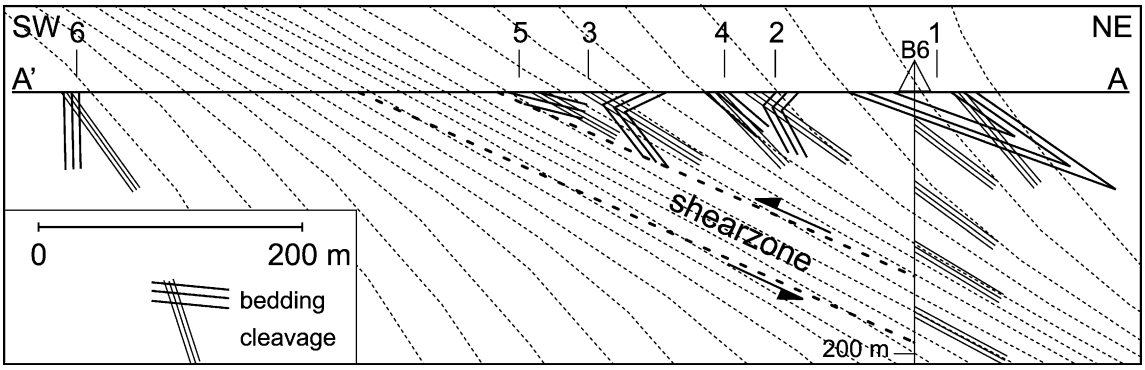

Fig. 3. Simplified cross-section through the outcrop area showing the sigmoidal change in cleavage dip and the probable orientation of the shear zone. Numbers refer to the outcrops and B6 to the location of borehole B6. The position of the profile is indicated in Fig. 2.

modation within the East Avalonia microcontinent related to the closure of the Rheic Ocean along the southern margin of East Avalonia (Pickering and Smith, 1995; Cocks et al., 1997; Rey et al., 1997). Mesozoic and Cenozoic cover sequence conceal to a large extent the Lower Palaeozoic basement. The outcrop area is localised along its southern margin, just north of the Hercynian (Givetian) unconformity. Exposures are limited to the upper courses of the tributaries of the Schelde and Meuse rivers and to a number of quarries.

The study area is situated in the valley of the Marcq river near Sint–Pieters–Kapelle. A detailed study of the outcrops in the area revealed the presence of a low-angle reverse shear zone (Debacker, 1999). However, its regional significance is yet unknown. A convergence at depth with the Asquempont Shear Zone is currently proposed (Sintubin, 1999). The Marcq area is situated on top of the gravimetric anomaly, suggesting the presence at depth of a granitoid body (Everaerts et al., 1996). The metasedimentary sequence in the Marcq area consists of an alternation of siltstones and pelites, reflecting a turbiditic environment. These metasediments belong to the Tremadocian Chevlipont Formation (Verniers et al., in press). Some volcanic horizons are intercalated in this formation. Although the magmatism in the southern Brabant Massif is considered of Ashgillian age (Van Grootel et al., 1997), the volcanic deposits in the Marcq area seem to be of Tremadocian age.

3. Methodology

Five boreholes have macroscopically been described and more than 200 samples have been taken for further petrographic, mineralogical and geochemical investigations. Thin sections were prepared to determine the mineralogy of the vein minerals, the alteration zones and the host rocks. Examination of polished surfaces led to the identification of the ore minerals and a detailed description of the paragenetic sequence. The mineralogy of the fine-grained crystals (e.g. sericite and other phyllosilicates) in the altered and unaltered rocks and along small faults was determined and quantified by X-ray diffraction using a Philips automated powder-diffraction system. Short-wave infrared (SWIR) reflected spectra were used to determine the phyllosilicate composition of samples from all five boreholes. A total of ~340 spectra, taken at an equidistance of 4 m, were collected using a PIMA-II device from Integrated Spectronics. This system operates in the SWIR-band between 1.3 and 2.5 μm with a spectral resolution of about 20 Å. Spectral processing, including adaptive noise removal Fourier filtering and unmixing procedures, was performed by Hunt Spectral Consultancy.

Doubly polished sections (300 μm thick) were prepared for the study of fluid inclusions in the gangue minerals. A detailed description of the sample preparation technique and of the measurement procedure has been given by Muchez et al. (1994). Microthermometric analyses of fluid inclusions were carried out on a fluid-adapted U.S.G.S. gas flow heating–freezing system, mounted on an Olympus BX60 microscope. Reproducibility was within 0.2 °C for

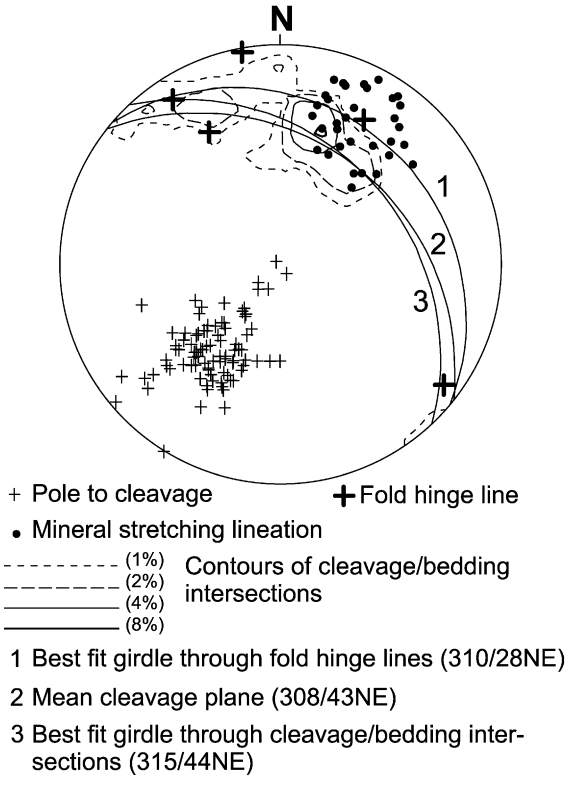

Fig. 4. Lower hemisphere equal-area stereographic projection showing the best-fit girdle through the fold hinge lines (girdle 1), the mean cleavage plane (girdle 2) and the best-fit girdle through the cleavage/bedding intersections (girdle 3).

the melting temperatures and <3 °C for the total homogenisation temperature ($T_{h\ Tot}$). Raman analyses have been made with a Dilor Microdil-28 multichannel Raman microspectrometre in the Institute of Earth Sciences, Vrije Universiteit Amsterdam, the Netherlands, using a 514-nm Ar-ion laser as source of excitation. The instrument and the measurement conditions have been described by Burke and Lustenhouwer (1987) and by Burke (2000).

The isotopic composition of quartz in veins ($\delta^{18}O$), fluid inclusions in vein quartz (δD) and sulphides ($\delta^{34}S$) was measured to determine the origin of the mineralising fluids. Quartz samples were selected based on their occurrence in the paragenetic sequence and hand picked. All separates were then analysed using a laser fluorination procedure, involving total sample reaction with excess ClF_3 using a CO_2 laser as a heat source. Reproducibility is better than 0.3 ‰ (1σ). Results were reported in standard notation ($\delta^{18}O$) as per mil (‰) deviations from the Standard Mean Ocean Water (V-SMOW) standard. Sulphides were prepared for isotopic analysis by standard heavy liquid, magnetic, diamond microdrilling and hand picking techniques. They were analysed by standard techniques

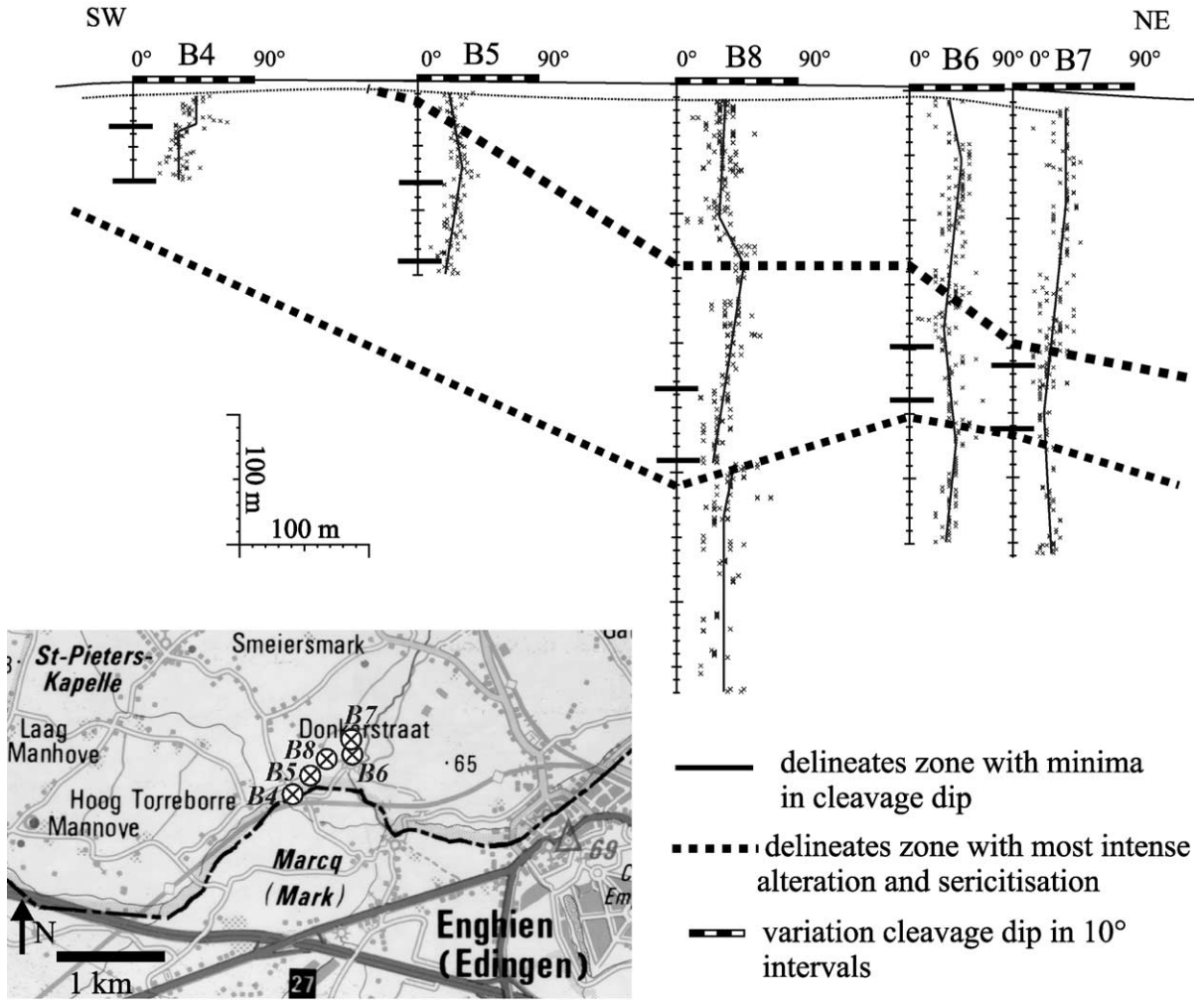

Fig. 5. Profile through the boreholes with macroscopically measured cleavage indicated in degrees (°). Borehole B8 is corrected for the deviation of the borehole. The core of alteration and sericitisation and the zones with the minima in the cleavage dip are indicated.

(Robinson and Kusakabe, 1975) in which SO_2 gas was liberated by combusting the sulphides with excess Cu_2O at 1075 °C in vacuo. Liberated gases were analysed on a VG Isotech SIRA II mass spectrometer. Reproducibility is better than 0.2‰ (1σ). Data are reported in $\delta^{34}S$ notation as per mil (‰) variations from the Canyon Diablo Troilite (CDT) standard. Samples selected for measurement of inclusion fluid δD were deemed suitable only if (a) they were 'clean' with regard to phases such as chlorite, micas and feldspar, and (b) dominated by a single type of fluid inclusions. The technique involves decrepitation of fluid inclusion in vacuo using bulk samples (>600 mg quartz) following the technique of Fallick et al. (1987). Data are reported in δD notation as per mil (‰) variations from the Standard Mean Ocean Water (V-SMOW) standard. Reproducibility of this procedure is around 5‰.

4. Structural analysis

Based on the aeromagnetic lineament map, the overall structural grain in the study area is NW–SE trending. The local structural geology of the Marcq area has been constrained by observations on six outcrops (Debacker, 1999) and corroborated with observations in the boreholes that are subject of the current study (Figs. 2 and 3).

The mean cleavage attitude (308/43NE, Figs. 3 and 4) coincides with the trend of the aeromagnetic lineaments in the area (Sintubin, 1997). Cleavage dip,

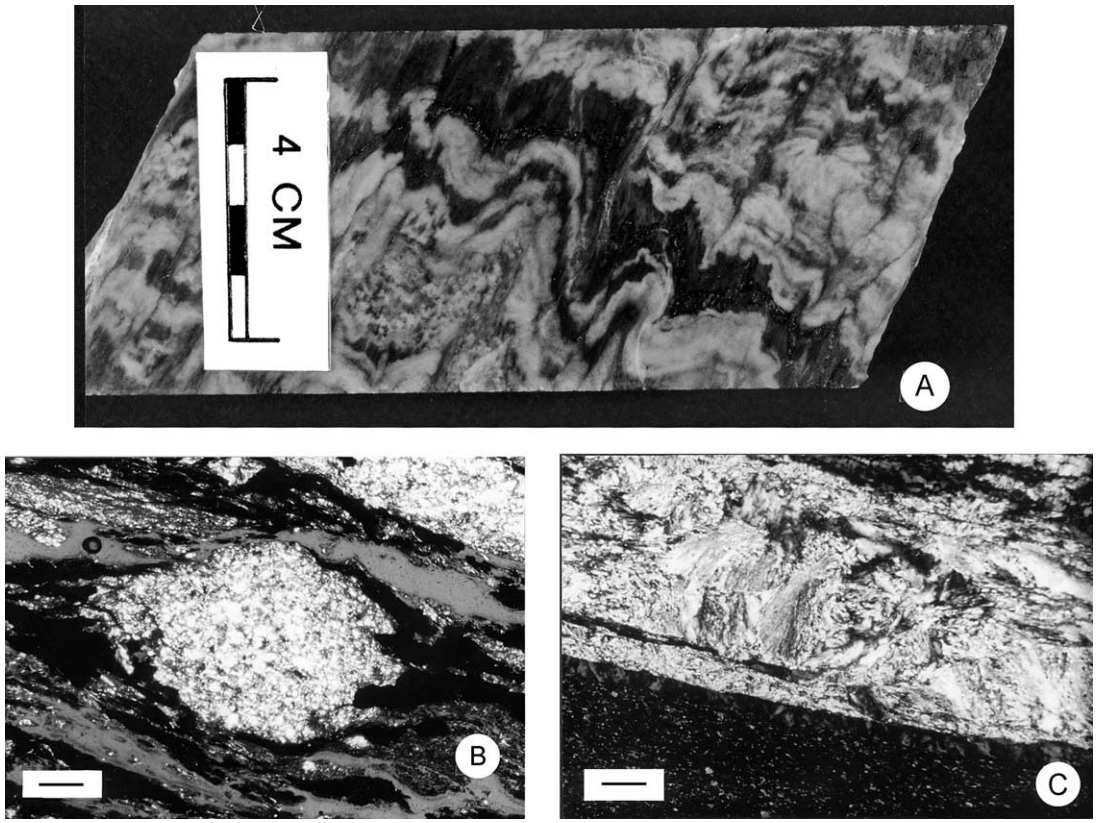

Fig. 6. (A) Photograph showing the pervasive cleavage present in the central part of shear zone. (B) Photomicrograph with typical σ-type winged quartz inclusions in a sericite matrix. (C) Curved muscovite fibres in a strain fringe, indicating a top-to-the-southwest displacement (top-to-right on photomicrograph). (B) and (C) with crossed polars. Scale bar is 135 μm.

however, shows a systematic variation along a profile perpendicular to the strike of the cleavage. Cleavage dip gradually decreases towards dips below 30° (Fig. 3). This gradual variation indicates a sigmoidal pattern. This sigmoidal pattern has also been observed in borehole B6 between 140 and 190 m depth (Debacker, 1999). Extrapolating towards the surface the zone with lowest cleavage dip should surface just southwest of outcrops 3 and 5 (Figs. 2 and 3). In order to check the regional presence of this sigmoidal cleavage pattern, 664 cleavage dips measured on non-oriented cores from the five boreholes (B4–B8) and covering a total length of 1410 m were reexamined (Fig. 2). Linear trends applied to parts of the data show that the cleavage dip changes 0.01–0.1°/m over intervals of 50 m or more. These gentle trends, together with the scattering of the results, require a statistical approach. Data were slightly smoothed by averaging them over 10-m intervals and were then divided into five quantiles which can be visualised using a grey scale. The pattern observed in Fig. 5 is clearly more complex than one sigmoidal variation, since several minima occur throughout each drilled section.

The central zone, with minimal cleavage dip, is moreover characterised by the most pervasive cleavage development (Fig. 6A), the occurrence of a down-dip stretching lineation and a pronounced sericitisation. Small-scale features, such as σ-type winged inclusions (Fig. 6B) and curved fibers in strain fringes (Fig. 6C), indicate a top-to-the-SW displacement. Based on the sigmoidal cleavage pattern, the strain localisation and the presence of shear sense indicators, the presence of a low-angle, NE-dipping reverse shear zone has been put forward (Debacker, 1999). The down-dip stretching lineation is interpreted to reflect the local tectonic transport direction (~ 210° EN).

Secondary folds, which developed largely coeval with the cleavage and, thus, the shear deformation, are typically asymmetric and non-cylindrical. The overall SW vergence corroborates the top-to-the-SW dis-

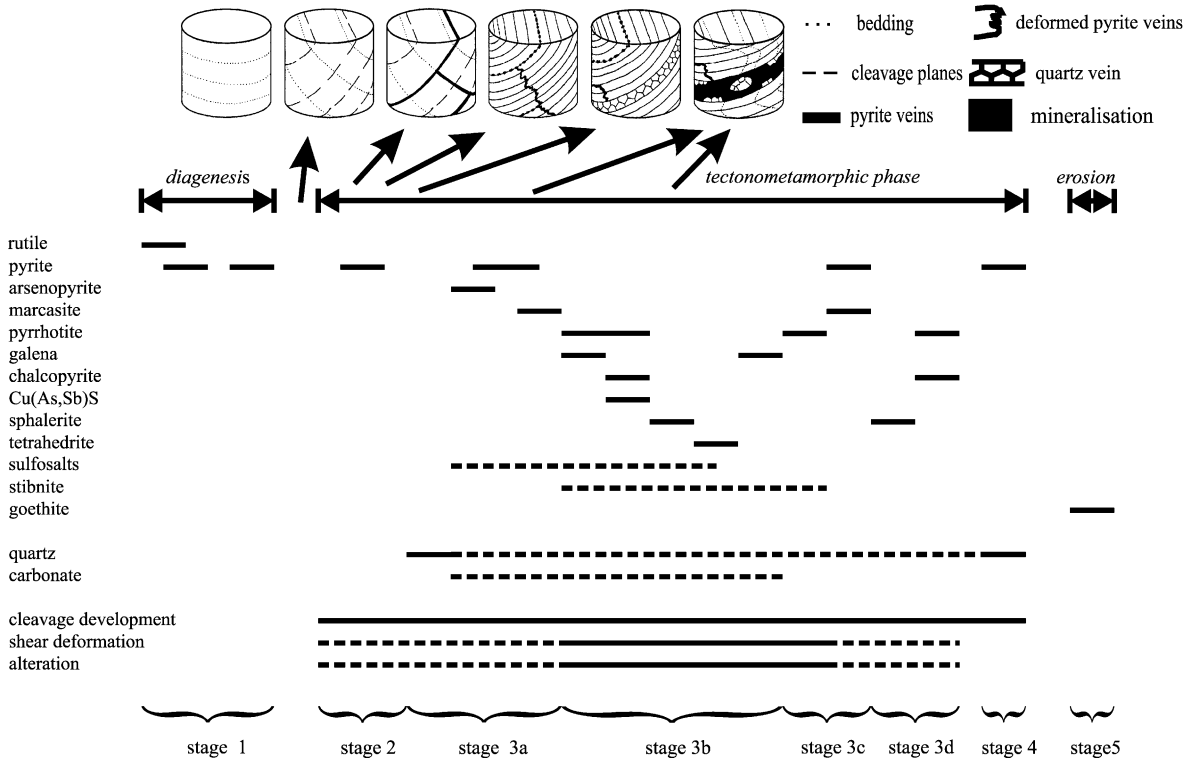

Fig. 7. Paragenesis of the mineralisation at Sint–Pieters–Kapelle with schematic illustration of the formation of some characteristic vein types. See text for explanation of stages 1–5.

placement. Fold hinge lines all lie within the cleavage plane, but are highly variable in trend and plunge (Fig. 2). This particular pattern of fold hinge lines is interpreted by Debacker (1999) to be caused by differential movement within the reverse shear zone, leading to NW–SE trending folds along the frontal tip line to NS or even NE–SW trending folds along lateral tip lines. The inferred presence of the tip line of the shear zone indicates that the displacement along the shear zone was minimal in the study area.

5. Petrography and mineral paragenesis

A polysulphide mineralisation is associated with the shear zone. Pyrite, marcasite, chalcopyrite, sphalerite, galena and stibnite are the main sulphide minerals. They occur in veins, often associated with quartz and diffusely distributed in the host rock. The mineralised veins are often oriented parallel to the cleavage. A detailed scheme of the mineral paragenesis is presented in Fig. 7. The paragenesis can be summarised in five main mineralising stages, which have a temporal link with the tectonic deformation.

The earliest sulphides (stage 1) consist of framboidal pyrites, which are probably synsedimentary or early diagenetic and not related to the main phase of mineralisation. The first mineralised veinlets (stage 2) are at most a few millimetres thick and form along (early stage) cleavage or parallel to bedding planes. Stage 2 pyrites also occur as individual crystals along cleavage planes. They are corroded and deformed and show a well-developed pressure shadow (Fig. 8A). The veins show an antitaxial growth of pyrite. These veins have subsequently been deformed, as indicated by small boudinage and fold structures. Stage 3 starts

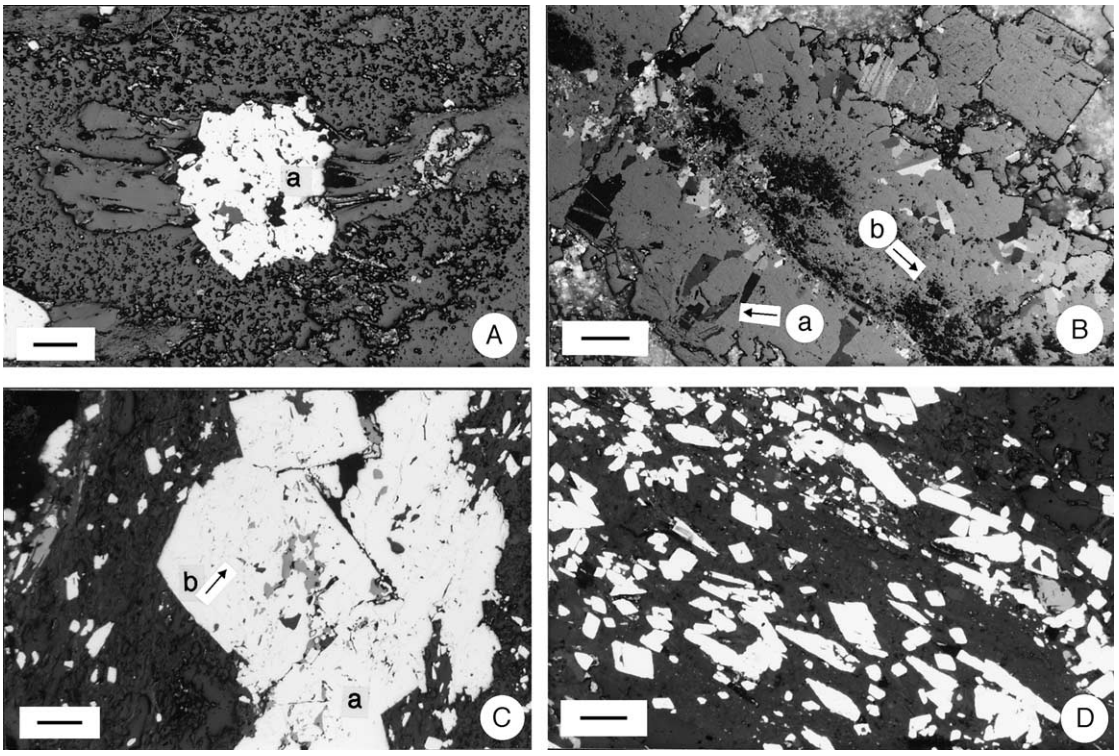

Fig. 8. (A) Corroded and deformed stage 2 pyrite (a) with a well-developed pressure shadow. Plane polarised light. Scale bar is 135 μm. (B) Polymorph of marcasite (a) after stage 2 pyrite and (b) in an antitaxial vein. Partly crossed nicols. Scale bar is 135 μm. (C) Pyrite (a) and enclosing arsenopyrite (b). Plane polarised light. Scale bar is 135 μm. (D) Arsenopyrite crystals oriented parallel to the cleavage. Shearing along the cleavage planes has deformed the crystals. Plane polarised light. Scale bar is 135 μm.

with the formation of quartz veins along the weakly dipping cleavage planes. The earliest-formed sulphides in stage 3 veins are pyrite, arsenopyrite, and marcasite (stage 3a; Fig. 8B and C). After their formation, extensive shear along the cleavage planes took place (Fig. 8D). Within these shear planes, sphalerite, chalcopyrite, galena, stibnite and minor pyrrhotite precipitated (stage 3b; Fig. 9A and B). Sphalerite, chalcopyrite, and galena are also found in pressure shadows around earlier pyrite grains, and are often intergrown with muscovite and/or chlorite (Fig. 9C and D). Also iron-rich calcite and siderite formed during this phase but they are less abundant. Stages 3c and d can only be recognised in the deepest part of B8. It starts with the formation of pyrrhotite, which is sometimes transformed to pyrite and marcasite. These are again corroded by polysulphides. In stage 4, quartz and pyrite precipitated in subvertical extension veins, with only limited evidence for deformation. Goethite probably has a more recent, secondary origin (stage 5).

6. Alteration and deformation patterns

The Lower Palaeozoic rocks in the Marcq area show chloritisation due to regional greenschist metamorphism (Van Grootel et al., 1997). In addition to this chloritisation, the mineralised zones in the boreholes underwent an intense silicification and sericitisation (Fig. 10A and B). Both these minerals and chlorite are also present as gangue minerals. Semiquantitative to quantitative changes in the phyllosilicate mineralogy with depth have been evaluated by X-ray diffraction and SWIR spectral analysis. The data show a strong

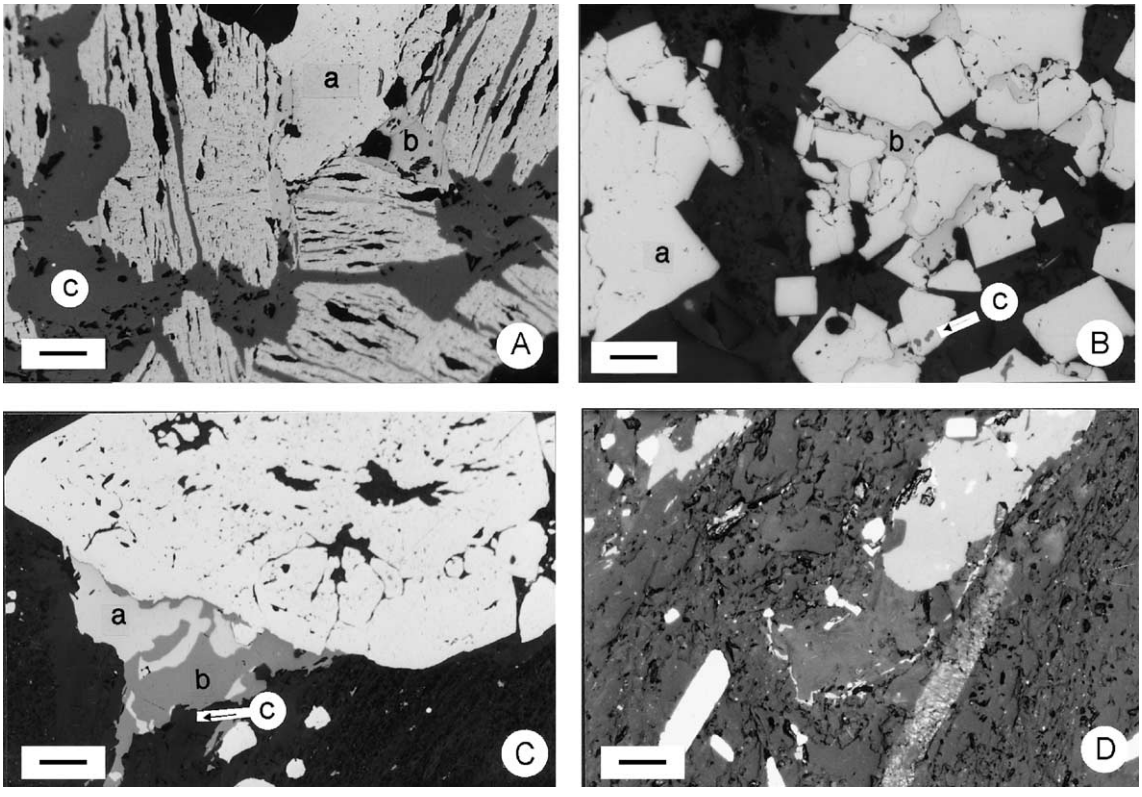

Fig. 9. (A) Marcasite (a) with bird's eye texture corroded by chalcopyrite (b) and sphalerite (c). Plane polarised light. Scale bar is 35 μm. (B) Cluster of pyrite crystals (a), which are fractured and corroded by chalcopyrite (b) and sphalerite (c). Plane polarised light. Scale bar is 133 μm. (C) Chalcopyrite (a) and sphalerite (b) intergrown with chlorite and muscovite (c) in a pressure shadow around pyrite. Plane polarised light. Scale bar is 135 μm. (D) Pressure shadow around deformed sphalerite. Plane polarised light. Scale bar is 135 μm.

variation in the muscovite and chlorite contents (Fig. 11). The unaltered rocks, that occur in the uppermost part of the Lower Palaeozoic at drill-sites B5 to B8, do not contain macroscopically recognisable sulphides, with the exception of pyrite. Downwards, the fabric changes due to silicification and sericitisation. The

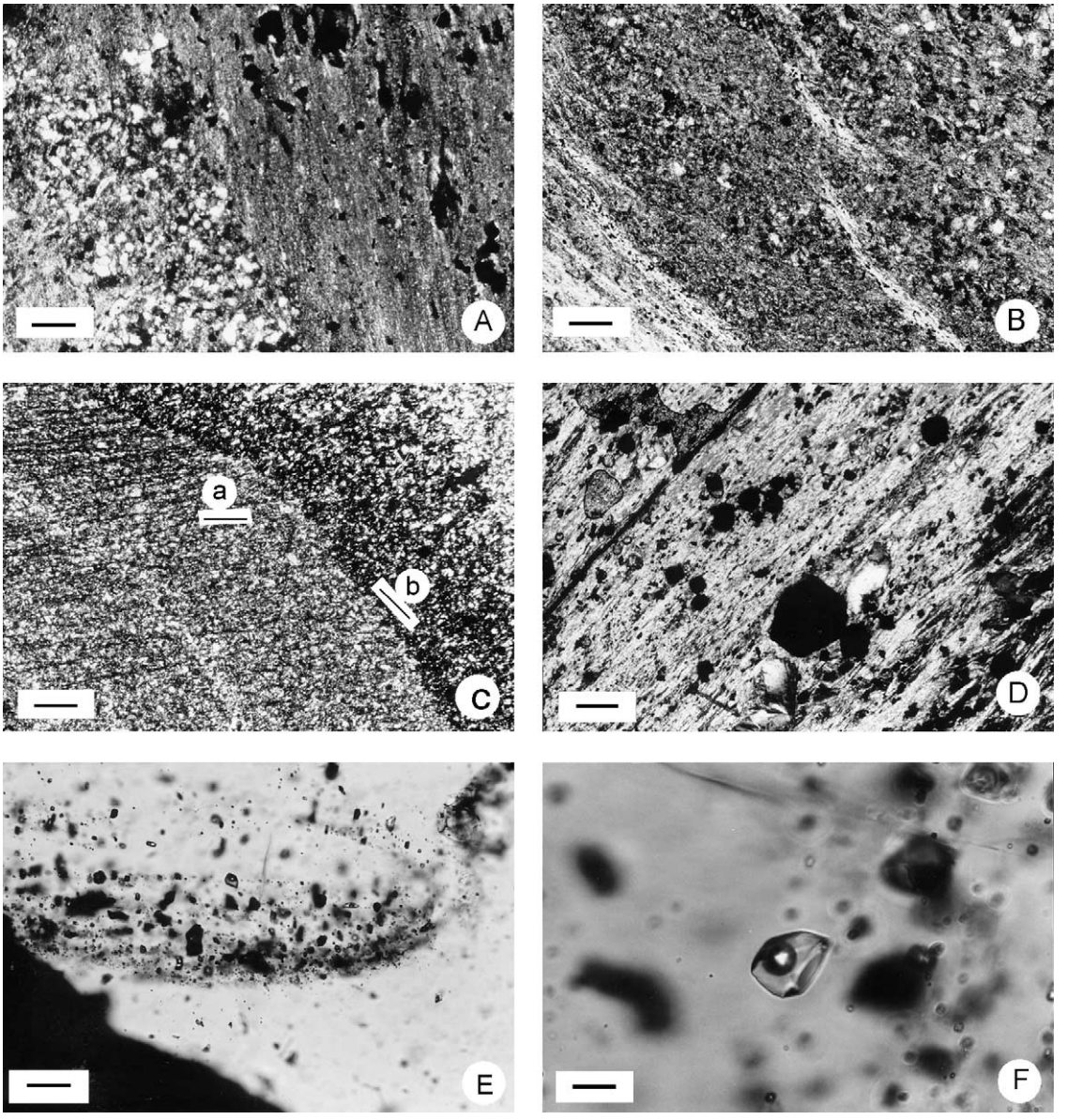

Fig. 10. (A) Layer of quartz with irregular crystal boundaries between intensely sericitised layers. The opaque minerals represent pyrite. Crossed nicols. Scale bar is 135 μm. (B) Intensely altered rock, mainly consisting of muscovite and quartz. Crossed nicols. Scale bar is 135 μm. (C) Clearly distinguishable cleavage (a), showing a low angle to the bedding (b). Crossed nicols. Scale bar is 135 μm. (D) Presence of pressure shadows around deformed pyrite (opaque minerals) parallel to the shear direction. Crossed nicols. Scale bar is 135 μm. (E) Secondary inclusions in quartz, which formed coeval with sulphide precipitation, characterised by the presence of two-phase aqueous–gaseous inclusions. Scale bar is 135 μm. (F) Detail of the trail showing two-phase aqueous–gaseous fluid inclusions. Scale bar is 135 μm.

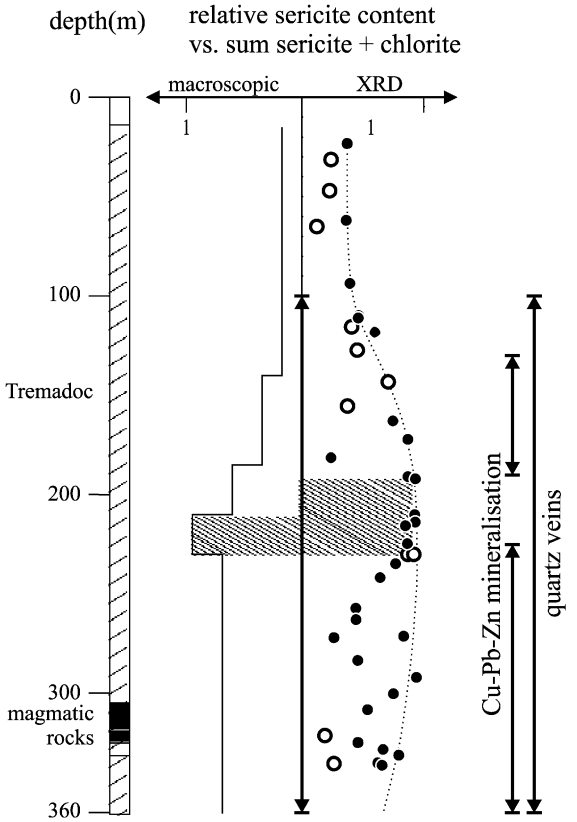

Fig. 11. Relative intensity of the sericitic alteration versus depth in borehole B7. The shaded area delineates the most strongly altered interval. The full and open circles correspond to the relative mineral compositions of host-rock and of the slickenfibers, respectively.

most strongly altered rocks, resembling talc, consist of fine-grained muscovite. Below these strongly altered rocks, silicification and a second phase of chloritisation become more important again. Since silicification is difficult to quantify, efforts to visualise alteration have been focused on the muscovite and chlorite content. Spatial visualisation of the SWIR-spectra shows a clearly delineated muscovite-rich zone, with an average relative muscovite content greater than 63 vol.%. These zones occur in the central parts of B6, B7, B8 and compose a large part of B4 and B5. The shallower and deeper rocks in B6 to B8 contain more chlorite. The non- to weakly altered rocks are characterised by a relatively high chlorite content. The width of the muscovite-rich zone is variable, and ranges between 70 and 200 m. The alteration pattern dips 0–30° to the NE in the profile formed by the five boreholes. This is in agreement with the general orientation of the shear zone proposed by Debacker (1999). The cleavage dips at a slightly steeper angle than both shear zone and alteration pattern.

Chlorite–muscovite slickenfibers on the cleavage planes formed during cleavage-parallel shear and are cogenetic with the Cu–Pb–Zn mineralisation, since the deformed ore minerals also occur along the cleavage. The variation in the mineralogy of the fibers is similar to the alteration pattern present in the host rocks, suggesting that sericitisation was associated with this period of deformation. In the boreholes, shear folds with a wavelength of a few decimetres can be observed. They are easily recognised where the strike of the cleavage and the stratification are parallel (Fig. 10C), but also occur where this relation is oblique. The shear fold geometry indicates dip-slip shear movement along the cleavage planes. The formation of these folds is coeval with the slickenfibers on the cleavage planes and with the Cu–Pb–Zn mineralisation and quartz precipitation (Fig. 10D). The sulphides are found as pressure shadows around other grains, or as deformed grains, parallel to the shear direction.

7. Microthermometry

Seventeen quartz veins that are considered to have been formed during stage 3 of the paragenesis were microthermometrically investigated. Primary inclusions in these veins are rare. However, textures such as fluid inclusions in recrystallisation rims of quartz related to other stage 3 minerals, and fluid inclusions in trails (Fig. 10E) associated with sulphide precipitation, allow the distinction of 256 inclusions which were trapped during stage 3 of the paragenesis. Fluid inclusions that formed later are present, but have not further been analysed in this study.

Microthermometry indicates that all early-formed inclusions are two-phase (L + V) aqueous–gaseous inclusions at room temperature (Fig. 10F). The temperature of melting of CO_2 ($T_{m\ CO_2}$) is between -69 and -56.6 °C (Fig. 12A). In a few inclusions, the eutectic melting temperature of the aqueous phase could be measured and is around -23 °C, indicative for the presence of KCl in addition to H_2O–NaCl (Shepherd et al., 1985). The ice-melting temperatures vary be-

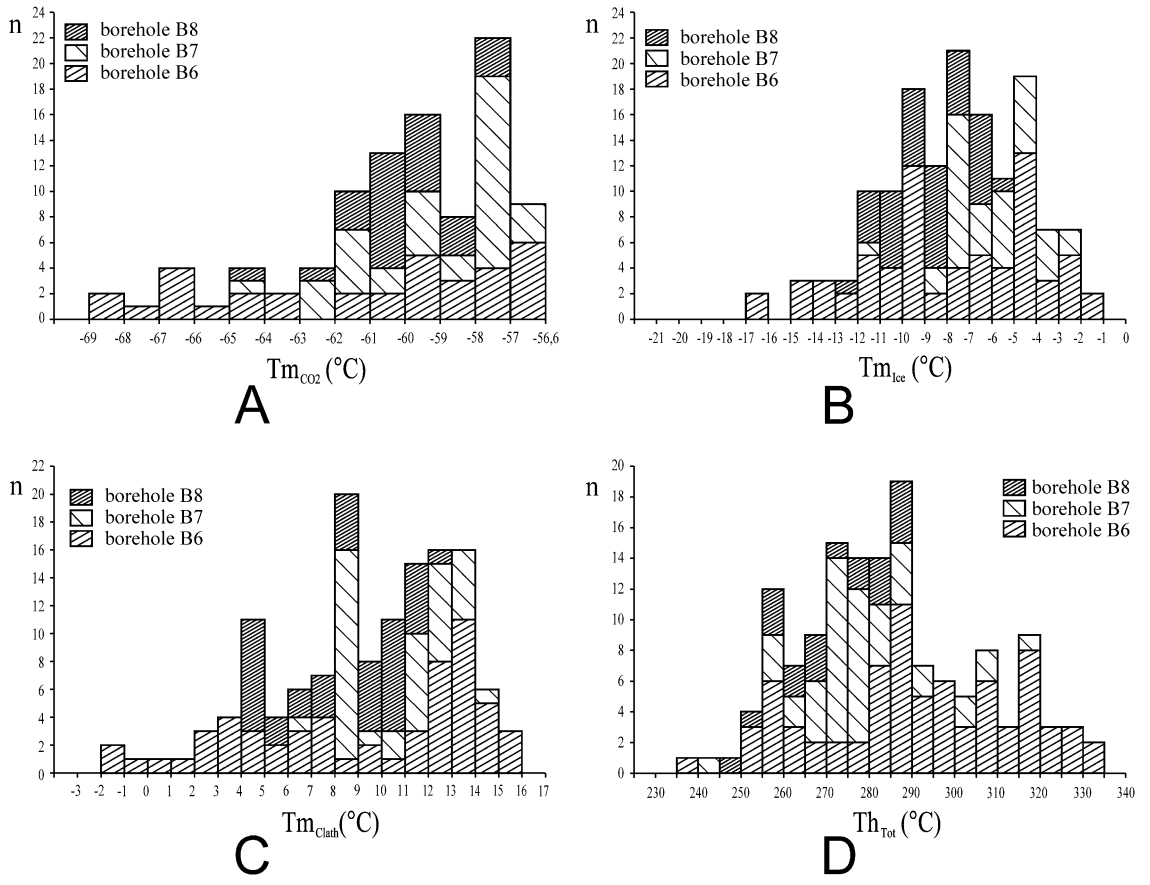

Fig. 12. Microthermometric data of aqueous–gaseous fluid inclusions in quartz associated with the polysulphide mineralisation (n = number of analyses). (A) Melting temperature of CO_2 ($T_{m\ CO_2}$). (B) Melting temperature of ice ($T_{m\ Ice}$). (C) Melting temperature of clathrate ($T_{m\ Clath}$). (D) Total homogenisation temperature ($T_{h\ Tot}$).

tween −1 and −17 °C with few values below −12 °C (Fig. 12B). The salinity of the fluid inclusions cannot be calculated from these ice-melting temperatures due to the removal of pure water during clathratation. Clathrate-dissociation temperatures ($T_{m\ Clath}$) can only be measured in the absence of a liquid CO_2 phase and are no longer a unique function of salinity. Although $T_{m\ Clath}$ values vary between −2 and +16 °C, most values occur between +6 and +14 °C (Fig. 12C). Most inclusions homogenise between 250 and 320 °C (Fig. 11D). Often, decrepitation occurs before total homogenisation and takes place above 250 °C. Raman spectroscopy shows the presence of CH_4 in addition to CO_2. No other gases have been detected. The CH_4 content in the inclusions measured by Raman spectroscopy ranges between 6 and 76 mol% (Table 1).

The $T_{m\ CO_2}$ values below −56.6 °C are, thus, due to the presence of CH_4. This gas also causes an increase in the chlathrate dissociation temperatures, which is also obvious from the $T_{m\ Clath}$ values above 10 °C, the chlathrate dissociation temperature in the H_2O–CO_2 system. Therefore, the primary two-phase aqueous–gaseous inclusions have an H_2O–CO_2–CH_4–NaCl–(KCl) composition. The salinity of the fluid inclusions has been calculated from the $T_{m\ Clath}$ values and the gas composition, as determined by Raman spectroscopy, using the computer program ICE of Bakker (1997) based on the equation of state of Duan et al. (1992a,b). The salinities of the inclu-

Table 1
Results of Raman spectroscopy of aqueous–gaseous fluid inclusions in quartz associated with the polysulphide mineralisation at Marcq (expressed in mole percent)

Sample	Inclusion	Percent CH_4	Percent CO_2
10990B6	1c	58	42
10990B6	3c	47	53
10990B6	3d	55	45
10990B6	2d	41	59
10990B6	4b	76	24
19100B7	2	44	56
19100B7	20	23	77
19100B7	23	20	80
19100B7	8	21	79
19100B7	14	35	65
19100B7	15	19	81
19100B7	1	41	59
19100B7	18	11	89
19100B7	19	27	73
23000B7	12	6	94
23000B7	5	6	94
23000B7	14	12	88
23000B7	19	9	91

sions for which both parameters are known lie between 1.6 and 7.3 eq. wt.% NaCl (Table 2).

Table 3
Results of stable isotope analyses of quartz ($\delta^{18}O$), fluid inclusions in quartz (δD) and sulphides ($\delta^{34}S$) in veins at Marcq

Sample	Mineral	$\delta^{18}O_{V\text{-}SMOW}$ (‰)	$\delta D_{V\text{-}SMOW}$ (‰)	$\delta^{34}S_{CDT}$ (‰)
03155B6	quartz	14.5	–	–
10985B6	sphalerite	–	–	8.0
10985B6	chalcopyrite	–	–	7.3
10985B6	pyrite	–	–	8.1
10985B6	pyrite	–	–	6.4
10990B6	quartz	13.2	− 35	–
12780B6	quartz	12.6	–	–
13245B6	pyrite	–	–	8.6
13260B6	quartz	13.3	− 50	–
13375B6	quartz	13.7	–	–
21670B6	quartz	12.5	–	–
23560B6	quartz	12.3	–	–
24070B6	quartz	12.3	–	–
19100B7	quartz	13.0	− 65	–
06815B8	quartz	13.2	− 39	–
06815B8	chalcopyrite	–	–	10.0
06815B8	marcasite	–	–	9.5
06815B8	sphalerite	–	–	8.3
06815B8	pyrite	–	–	9.8
21670B8	quartz	12.5	–	–

V-SMOW: Vienna standard mean ocean water, CDT: Canyon Diablo meteorite troilite.

8. Stable isotope analyses

Eleven quartz veins have been selected for stable isotope analyses. Seven of these veins are syntectonic (stage 3) and four are late-syntectonic (stage 4). The isotopic composition of all quartz veins ($\delta^{18}O$), of fluid inclusions in four vein quartz (δD) and of nine sulphides ($\delta^{34}S$) was measured to determine the origin of

Table 2
Calculated compositions of the $H_2O-CO_2-CH_4-NaCl-(KCl)$ inclusions

Sample	Inclusion	Total inclusion						Aqueous solution	
		Density (g/cm^3)	Molar volume (cm^3/mol)	H_2O (mol%)	CO_2 (mol%)	CH_4 (mol%)	NaCl (mol%)	NaCl (molality)	NaCl (massa%)
10990B6	4b	0.697	36.53	86.3	3.6	8.8	0.62	0.40	2.3
10990B6	1c	0.697	27.45	87.9	5.4	5.7	0.47	0.30	1.7
10990B6	3c	0.685	28.05	88.4	6.0	3.9	0.79	0.50	2.9
10990B6	2d	0.704	27.89	88.3	7.1	3.7	0.44	0.28	1.6
10990B6	3d	0.660	28.41	89.7	4.6	3.8	1.00	0.62	3.6
19100B7	1	0.772	24.68	90.3	5.4	2.5	0.87	0.53	3.1
19100B7	2	0.769	24.75	91.2	5.0	2.5	0.62	0.38	2.2
19100B7	8	0.763	25.15	90.2	6.3	1.1	1.19	0.73	4.3
19100B7	14	0.676	28.62	89.4	6.5	2.5	0.83	0.51	3.0
19100B7	15	0.891	21.85	90.3	6.9	1.1	0.87	0.54	3.1
19100B7	18	0.668	29.40	89.9	7.6	0.6	0.94	0.58	3.4
19100B7	19	0.667	28.98	89.3	6.7	1.7	1.14	0.71	4.2
19100B7	20	0.735	26.68	89.8	7.2	1.5	0.71	0.44	2.6
23000B7	14	0.725	25.80	90.0	5.5	0.4	2.02	1.25	7.3
23000B7	19	0.731	25.82	90.3	5.8	0.3	1.79	1.10	6.4

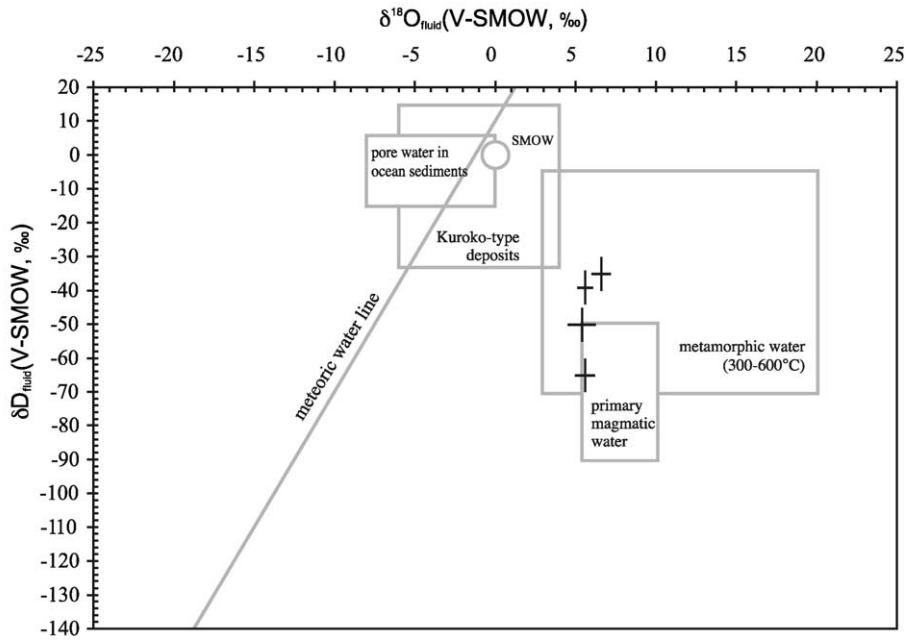

Fig. 13. Calculated $\delta^{18}O$ values and δD values of the mineralising fluids, indicated by crosses and the isotopic fields of metamorphic and primary magmatic fluids and volcanic-associated massif sulphide (Kuroko type) deposits (after Yurtsever and Gat, 1981; Pisutha-Arnond and Ohmoto, 1983; Ohmoto, 1986; Sheppard, 1986).

the mineralising fluids (Table 3). The analysed sulphides belong to stages 2, 3a, 3b and 4. To calculate the $\delta^{18}O$ and $\delta^{34}S$ compositions of the ambient fluids, the formation temperatures of the quartz veins and the associated sulphides have to be known. The precipitation temperature can be estimated from the homogenisation temperature of the fluid inclusions in the quartz veins. For the sulphides, a temperature has been assumed similar to that of the quartz vein in which they occur. The temperatures used are the mean homogenisation temperatures with a deviation of 2σ. These are of course only estimates, however, the presence of marcasite in phase 2a suggests that this could not be much higher (Murowchick and Barnes, 1986; Piessens et al., 1999). If the precipitation temperature was 100 °C higher, the $\delta^{18}O$ values increase by less than 4 ‰ and $\delta^{34}S$ by less than 0.5 ‰.

The calculated oxygen ($\delta^{18}O$) and sulphur ($\delta^{34}S$) isotopic compositions of the ambient fluid fall, respectively, between +3 ‰ and +8 ‰ V-SMOW and between +4.7 ‰ and +10.6 ‰ CDT. In a $\delta^{18}O-\delta D$ plot (Fig. 13), the values cluster in the field typical for metamorphic fluids and partly overlap with that for primary magmatic fluids (Fig. 13). The $\delta^{34}S$ values (Fig. 14) fall outside the interval typical for I-type magmas (−3 ‰ to +3 ‰ CDT; Ohmoto and Rye, 1979; Ohmoto, 1986).

9. Discussion

In the boreholes studied, the polysulphide mineralisation zones are restricted to the altered intervals. The mineralising and altering fluids must have followed the same migration pathways. This close relationship is further confirmed by the association of chalcopyrite, sphalerite and galena with muscovite and chlorite in veins. The cleavage-parallel orientation of the mineralised veins and the subsequent deformation of the sulphides in these veins demonstrate that the mineralisation took place during a protracted simple shear deformation in which cleavage planes are reactivated as shear planes. The composition of the minerals, along these reactivated cleavage planes, shows the same evolution in the sericite–chlorite pattern as the surrounding altered host rocks. These two arguments suggest

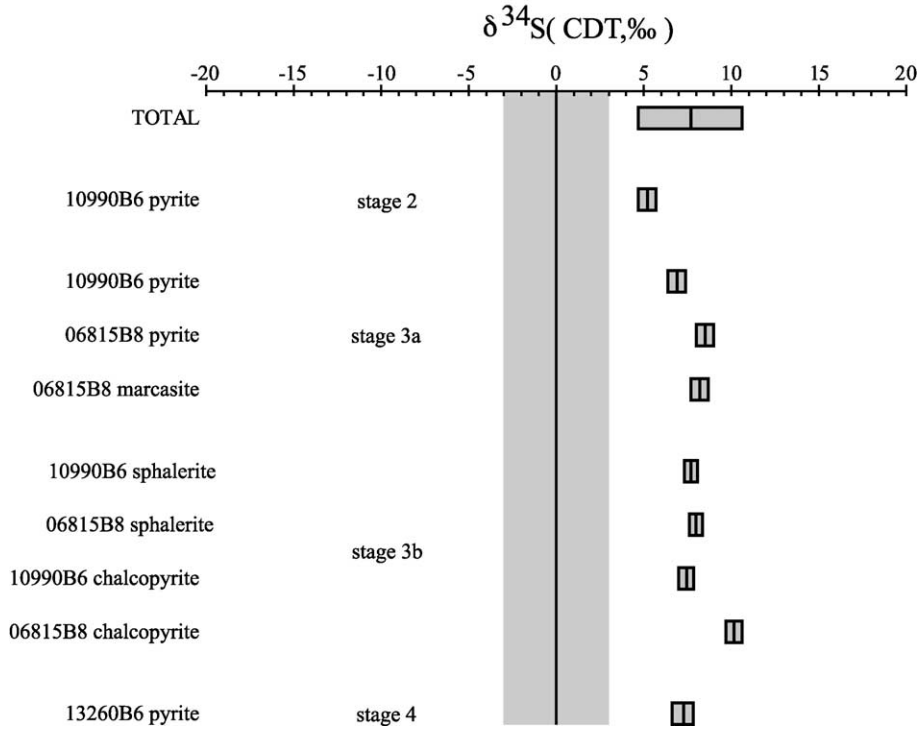

Fig. 14. δ^{34}S values of the sulphides in the mineralisation associated with the shear zone. The rectangles indicate the calculated values (middle line) with the level of significance, based on the error of the measurement and the formation temperature. Shaded area indicates the range typical for I-type magmas.

that alteration and deformation were also coeval. Therefore, mineralisation, alteration and deformation occurred largely during the same progressive deformation event, slightly post-dating the development of the cleavage fabric. Since at present there is only evidence for one single major deformation event in the Brabant Massif, occurring during the early Devonian, it is proposed that precipitation of the polysulphides occurred during the final stages of this deformation event.

The alteration pattern, evident from the relative abundance of muscovite and chlorite, shows well-defined low-angle NE-dipping alteration zones (Fig. 15). Such a well-defined pattern indicates a strong control on the hydrothermal migration of the fluids. Regarding the structural setting, the NE-dipping shear zone forms an ideal structural feature in focussing the upward migration of the mineralising fluids. Since the zones with the lowest cleavage dip, present in the sericite-rich rocks, do not line up along one plane, it is unlikely that the shear zone is a narrow and well-defined structure. Therefore, a broader anastomosing shear zone is proposed, in which strain localisation occurred in a more irregular way (Fig. 15).

The mineralising fluids have an $H_2O-CO_2-CH_4-NaCl-(KCl)$ composition, a low salinity (2–7 eq. wt.% NaCl) and temperatures above 250 °C. These characteristics are comparable with the Phanerozoic polysulphide and gold mineralisation in the Caledonides of the British Isles (Mason, 1997; Steed and Morris, 1997; Lowry et al., 1997). The ore deposits in these areas are often associated with granitic intrusions. In addition, magmatic rocks are present in the Brabant Massif. Except for the magmatic rocks in the study area itself, magmatic activity (rhyodacitic and andesitic) in the Brabant Massif is mostly restricted to the Ashgillian (late Ordovician), with some minor evidence of volcanism during the Llandovery (early Silurian). This indicates that volcanism preceded the early Devonian mineralisation by at least 30 Ma. Magmatic fluids can therefore be ruled out as the dominant

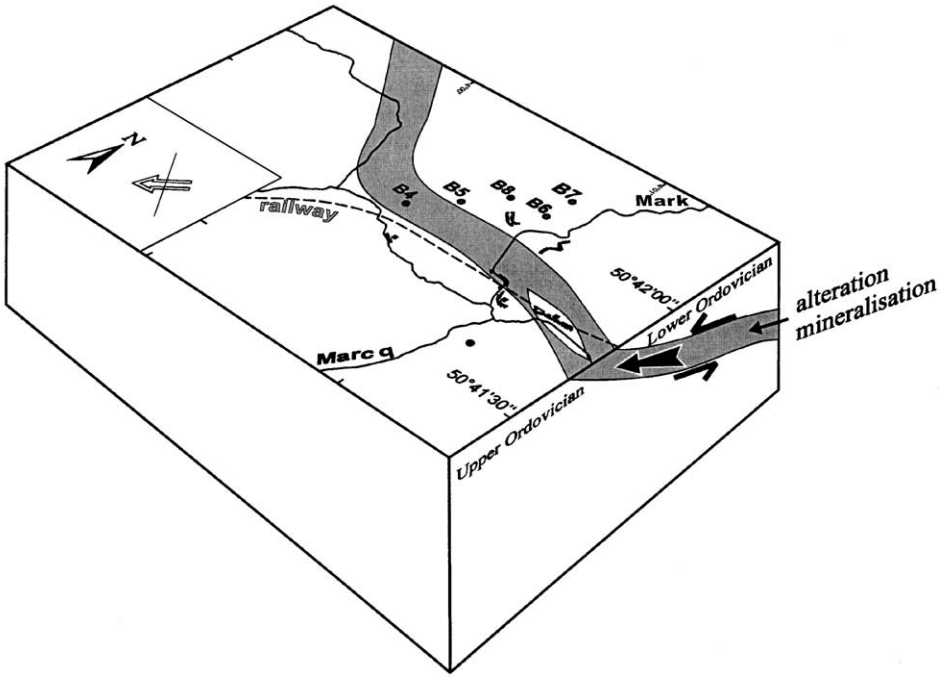

Fig. 15. Schema of the shear zone. The NE-dipping zone of alteration and mineralisation with the position of the boreholes is indicated.

source or transport medium for the mineralisation. The alternative explanation, involving mainly metamorphic fluids, is in complete agreement with the tectonometamorphic framework of the mineralisations.

The source rocks for the metamorphic fluids could theoretically be I- or S-type magmatic or sedimentary rocks. Since only part of the $\delta^{18}O$ and δD data and none of the $\delta^{34}S$ correspond to I-type magmatic rocks, these can be regarded as a less likely source. Isotope data are compatible with both S-type magmatic and metamorphic fluids. However, the volume of volcanic rocks is relatively small compared to the volumes needed to produce sufficient fluids for the mineralisation. Therefore, fluids are interpreted to have been expelled during metamorphic reactions within clastic sediments. In addition, the presence of CH_4 in the fluid inclusions, resulting from the breakdown of organic material, is a good indication of this metamorphic origin.

To our knowledge, no other study has demonstrated in detail a close spatial and temporal relationship between alteration, polysulphide mineralisation and the early Devonian deformation in the Brabant Massif. Extensive migration of metamorphic fluids accompanied progressive deformation along a low-angle reverse shear zone. The structural setting of the Marcq area is unique. Most probably, the presence of a rigid granitoid body at depth inhibited the southward-migrating deformation causing thrusting in the hanging wall of the granitoid basement block. Sintubin (1999) proposed that several thrusts, like the one identified in the Marcq area, root into the Asquempont Shear Zone, bordering the central steep belt to the SW. A larger-scale structural and geochemical study of the veining associated with the Asquempont Shear Zone will elucidate if a common fluid flow system is present. Such a study will eventually allow putting the results of the current study in the Marcq area into the broader perspective of the tectonic history at the southern extremity of the Anglo-Brabant fold belt.

10. Conclusions

The intense alteration and polysulphide mineralisation in the Lower Palaeozoic rocks of the Brabant Massif in the Marcq area are spatially associated with a low-angle, NE-dipping shear zone. Temporarily, it is related to a shear reactivation of the cleavage planes,

indicative of a progressive simple shear deformation history. The zone of alteration and mineralisation extends over a maximum thickness of 250 m, that corresponds to the maximum thickness of the anastomosing shear zone. The ambient fluids, with an H_2O–CO_2–CH_4–NaCl–(KCl) composition and minimum temperatures of 250–320 °C, most likely had a metamorphic origin. They caused the precipitation of the sulphide minerals and the sericitisation and silicification of the host rock. Although from a tectonic point of view of local significance, the evidence of extensive migration of metamorphic fluids along shear zones during the early Devonian deformation event in the Brabant Massif has to be reckoned with when establishing the tectonic history in the Anglo-Brabant fold belt.

Acknowledgements

We are grateful to Patrick Ledru and an anonymous reviewer for their constructive and thoughtful review. ANRE (Division of Natural Resources and Energy) of the Flemish Community, under supervision of its former division head P. Vansteelandt, funded this 3-year project. Additional funding was provided by the Fund of Scientific Research of Flanders (F.W.O.-Vlaanderen, Belgium) project G.0274.99. The cores studied are the property of the company Terex and the Flemish community. We are grateful to both for permission to publish the results. We also thank J. Coppens-Vander Auwera, editor of Geologica Belgica, for the permission to reproduce figures from the paper published by Debacker in Geologica Belgica. Herman Nijs carefully prepared thin sections and the doubly polished wafers. SWIR spectra were measured using the PIMA-II device, put at our disposal by F. van der Meer and P. van Dijk from the ITC (The Netherlands), who also assisted in the interpretation of the results. Manuel Sintubin and Timothy Debacker are, respectively, Postdoctoral Fellow and Research Assistant of the F.W.O.-Vlaanderen (Belgium).

References

André, L., Deutsch, S., Michot, J., 1981. Données géochronologiques concernant le développement tectono-métamorphique du segment Calédonien Brabançon. Ann. Soc. Geol. Belg. 104, 241–253.

Bakker, R.J., 1997. Clathrates: computer programs to calculate fluid inclusion V–X properties using clathrate melting temperatures. Comput. Geosci. 23, 1–18.

Blundell, D.J., Freeman, R., Mueller, S., 1992. A continent revealed. The European Geotraverse. Cambridge Univ. Press, Cambridge.

Bottrell, S.H., Shepherd, T.J., Yardley, B.W.D., Dubessy, J., 1988. A fluid inclusion model for the genesis of the ores of the Dolgellau Gold Belt, North Wales. J. Geol. Soc. (London) 145, 139–145.

Burke, E.A.J., 2000. Raman microspectrometry of fluid inclusions. Lithos 55, 139–158.

Burke, E.A.J., Lustenhouwer, W.J., 1987. The application of a multichannel laser Raman microprobe (Microdil-28®) to the analysis of fluid inclusions. Chem. Geol. 61, 11–17.

Chacksfield, B.C., De Vos, W., D'Hooge, L., Dusar, M., Lee, M.K., Poitevin, C., Royles, C.P., Verniers, J., 1993. A new look at Belgian aeromagnetic and gravity data through image-based display and integrated modelling techniques. Geol. Mag. 130, 583–591.

Cocks, L., McKerrow, W., Van Staal, C., 1997. The margins of Avalonia. Geol. Mag. 134, 627–636.

Cox, S.F., Wall, V.J., Etheridge, M.A., Potter, T.F., 1991. Deformational and metamorphic processes in the formation of mesothermal vein-hosted gold deposits—examples from the Lachlan Fold Belt in central Victoria, Australia. Ore Geol. Rev. 6, 391–423.

Craw, D., Windle, S.J., Angus, P.V., 1999. Gold mineralization without quartz veins in a ductile–brittle shear zone, Macraes Mine, Otago Schist, New Zealand. Miner. Deposita 34, 382–394.

Debacker, T.N., 1999. Folds trending at various angles to the transport direction in the Marcq area, Brabant Massif, Belgium. Geol. Belg. 2, 159–172.

Debacker, T.N., Sintubin, M., Verniers, J., 1999. Cleavage/fold relationships in the Silurian metapelites, southeastern Anglo-Brabant fold belt (Ronquières, Belgium). Geol. Mijnbouw 78, 47–56.

De Vos, W., Verniers, J., Herbosch, A., Vanguestaine, M., 1993. A new geological map of the Brabant Massif, Belgium. Geol. Mag. 130, 605–611.

Duan, Z., Möller, N., Weare, J.H., 1992a. An equation of state for the CH_4–CO_2–H_2O system: I. Pure systems from 0 to 1000 °C and 0 to 8000 bar. Geochim. Cosmochim. Acta 56, 2605–2617.

Duan, Z., Möller, N., Weare, J.H., 1992b. An equation of state for the CH_4–CO_2–H_2O system: II. Mixtures from 50 to 1000 °C and 0 to 1000 bar. Geochim. Cosmochim. Acta 56, 2605–2617.

Duller, P.R., Gallagher, M.J., Hall, A.J., Russell, M.J., 1997. Glendinning deposit—an example of turbidite-hosted arsenic–antimony–gold mineralization in the Southern Uplands, Scotland. Trans. Inst. Min. Metall., Sect. B: Appl. Earth Sci. 106, 119–134.

Everaerts, M., Poitevin, C., De Vos, W., Sterpin, M., 1996. Integrated geophysical/geological modelling of the western Brabant Massif and structural implications. Bull. Soc. Belge Geol. 105, 41–59.

Fallick, A.E., Jocely, J., Hamilton, P.J., 1987. Oxygen and hydrogen stable isotope systematics in Brazilian agates. In: Rodriquez Clemente, E. (Ed.), Geochemistry of the Earth Surface and Processes of Mineral Formation. Instituto de Geologica (CSIC), Madrid, pp. 99–117.

Groves, D.I., 1993. The crustal continuum model for late-Archean lode-gold deposits of the Yilgarn Block, Western Australia. Miner. Deposita 28, 366–374.

Huizenga, J.M., 1995. Fluid evolution in shear zones from the late Archean Harare-Shamva-Bindura greenstone belt (NE Zimbabwe): thermodynamic calculations of the C-O-H system applied to fluid inclusions. PhD thesis, Vrije Universiteit Amsterdam, The Netherlands.

Ixer, R.A.F., Pattrick, R.A.D., Stanley, C.J., 1997. Geology, mineralogy and genesis of gold mineralization at Calliachar-Urlar Burn, Scotland. Trans. Inst. Min. Metall., Sect. B: Appl. Earth Sci. 106, 99–108.

Kerrich, R., 1987. The stable isotope geochemistry of Au–Ag vein deposits in metamorphic rocks. In: Kyser, T.K. (Ed.), Stable Isotope Geochemistry of Low Temperature Fluids. Mineral. Assoc. Canada Short Course Handbook, vol. 13, pp. 287–336.

Kyser, T.K., Kerrich, R., 1990. Geochemistry of fluids in tectonically active crustal regions. In: Nesbitt, B.E. (Ed.), Fluids in Tectonically Active Regimes of the Continental Crust. Mineral. Assoc. Canada Short Course, Handbook, vol. 18, pp. 133–230.

Legrand, R., 1967. Ronquières. Documents géologiques. Mem. Cartes Geol. Miner. Belg. 6, 1–60.

Lowry, D., Boyce, A.J., Fallick, A.E., Stephens, W.E., 1997. Sources of sulphur, metals and fluids in granitoid-related mineralization of the Southern Uplands, Scotland. Trans. Inst. Min. Metall., Sect. B: Appl. Earth Sci. 106, 157–168.

Mansy, J.L., Everaerts, M., De Vos, W., 1999. Structural analysis of the adjacent Acadian and Variscan fold belts in Belgium and Northern France from geophysical and geological evidence. Tectonophysics 309, 99–116.

Mason, J.S., 1997. Regional polyphase and polymetallic vein mineralization in the Caledonides of the Central Wales Orefield. Trans. Inst. Min. Metall., Sect. B: Appl. Earth Sci. 106, 135–143.

Muchez, Ph., Marshall, J.D., Touret, J.L.R., Viaene, W.A., 1994. Origin and migration of palaeofluids in the Upper Viséan of the Campine Basin, northern Belgium. Sedimentology 41, 133–145.

Muir-Wood, R., King, G., 1993. Hydrological signatures of earthquake strain. J. Geophys. Res. 98, 22035–22068.

Murowchick, J.B., Barnes, H.L., 1986. Marcasite precipitation from hydrothermal solutions. Geochim. Cosmochim. Acta 50, 2615–2629.

Murphy, P.J., Roberts, S., 1997. Evolution of a metamorphic fluid and its role in lode gold mineralisation in the Central Iberian Zone. Miner. Deposita 32, 459–474.

Nesbitt, B., Muehlenbachs, K., 1989. Origins and movement of fluids during deformation and metamorphism in the Canadian Cordillera. Science 245, 733–736.

Nguyen, P.T., Cox, S.F., Harris, L.B., Powell, Ch. McA., 1998. Fault-valve behaviour in optimally oriented shear zones: an example at Revenge gold mine, Kambalda, Western Australia. J. Struct. Geol. 20, 1625–1640.

Ohmoto, H., 1986. Stable isotope geochemistry of ore deposits. In: Valley, J.W., Taylor, H.P., O'Neil, J.R. (Eds.), Stable Isotopes in High Temperature Geological Processes. Rev. Mineral. 16, 419–559.

Ohmoto, H., Rye, R.O., 1979. Isotopes of sulfur and carbon. In: Barnes, H.L. (Ed.), Geochemistry of Hydrothermal Ore Deposits. Wiley, New York, pp. 509–567.

Pettke, T., Diamond, L.W., Villa, I.M., 1999. Mesothermal gold veins and metamorphic devolatilization in the northwestern Alps: the temporal link. Geology 27, 641–644.

Pharaoh, T.C., England, R., Lee, M.K., 1995. The concealed Caledonide basement of eastern England and the southern North Sea—a review. Stud. Geophys. Geod. 39, 330–346.

Pickering, K.T., Smith, A.G., 1995. Arcs and backarc basins in the Early Paleozoic Iapetus Ocean. Isl. Arc 4, 1–67.

Piessens, K., Muchez, Ph., Viaene, W., De Vos, W., 1999. Syntectonic polysulphide mineralisation in the Brabant Massif, Belgium. In: Stanley, C. (Ed.), Mineral Deposits: Processes to Processing. Balkema, Rotterdam, The Netherlands, pp. 963–966.

Pisutha-Arnond, V., Ohmoto, H., 1983. Thermal history, and chemical and isotopic compositions of the ore-forming fluids responsible for the Kuroko massive sulfide deposits in the Hokuroku district of Japan. In: Ohmoto, H., Skinner, B.J. (Eds.), The Kuroko and Related Volcanogenic Massive Sulfide Deposits. Economic Geology Monograph 5, 523–558.

Rey, P., Burg, J.-P., Casey, M., 1997. The Scandinavian Caledonides and their relationship to the Variscan belt. In: Burg, J.-P., Ford, M. (Eds.), Orogeny Through Time. Geol. Soc. London, Spec. Publ. 121, 179–200.

Robert, F., Boullier, A.-M., Firdaous, K., 1995. Gold–quartz veins in metamorphic terrains and their bearing on the role of fluids in faulting. J. Geophys. Res. 100, 12861–12879.

Roberts, R.G., 1987. Ore deposit models # 11. Archaean lode gold deposits. Geosci. Can. 14, 37–51.

Robinson, B.W., Kusakabe, M., 1975. Quantitative preparation of SO_2 for $^{34}S/^{32}S$ analysis from sulfides by combustion with cuprous oxide. Anal. Chem. 47, 1179–1181.

Shepherd, T.J., Rankin, A.H., Alderton, D.H.M., 1985. A practical guide to fluid inclusions studies. Blackie, London.

Sheppard, S.M.F., 1986. Characterization and isotopic variations in natural waters. In: Valley, J.W., Taylor, H.P., O'Neil, J.R. (Eds.), Stable Isotopes in High Temperature Geological Processes. Rev. Mineral. 16, 165–183.

Sibson, R., 1994. Crustal stress, faulting and fluid flow. In: Parnell, J. (Ed.), Geofluids: Origin, Migration and Evolution of Fluids in Sedimentary Basins. Geol. Soc. Spec. Publ., vol. 78, pp. 69–84.

Sibson, R.H., Robert, F., Poulsen, K.H., 1988. High-angle reverse faults, fluid pressure cycling and mesothermal gold–quartz deposits. Geology 16, 551–555.

Sintubin, M., 1997. Cleavage–fold relationships in the Lower Paleozoic Brabant Massif (Belgium). Aardk. Meded. Univ. Leuven 8, 161–164.

Sintubin, M., 1999. Arcuate fold and cleavage patterns in the southeastern part of the Anglo-Brabant Fold belt (Belgium): tectonic implications. Tectonophysics 309, 81–97.

Sintubin, M., Brodkom, F., Laduron, D., 1998. Cleavage–fold relationship in the Lower Cambrian Tubize Group, southeast Anglo-Brabant Fold Belt. Geol. Mag. 135, 217–226.

Steed, G.M., Morris, J.H., 1997. Isotopic evidence for the origins of a Caledonian gold–arsenopyrite–pyrite deposit at Clontibret, Ireland. Trans. Inst. Min. Metall., Sect. B: Appl. Earth Sci. 106, 109–118.

Teagle, D.A.H., Norris, R.J., Craw, D., 1990. Structural controls on gold-bearing quartz mineralization in a duplex thrust system, Hyde–Macreas Shear zone, Otago schist, New Zealand. Econ. Geol. 85, 1711–1719.

Touray, J.-C., Marcoux, E., Hubert, P., Proust, D., 1989. Hydrothermal processes and ore-forming fluids in the Le Bourneix gold deposit, central France. Econ. Geol. 84, 1328–1339.

Travé, A., Calvet, F., Soler, A., Labaume, P., 1998. Fracturing and fluid migration during Palaeogene compression and Neogene extension in the Catalan Coastal Ranges, Spain. Sedimentology 45, 1063–1082.

Van Grootel, G., Verniers, J., Geerkens, B., Laduron, J., Verhaeren, M., Hertogen, J., De Vos, W., 1997. Timing of magmatism, foreland basin development, metamorphism and inversion in the Anglo-Brabant fold belt. Geol. Mag. 134, 607–616.

Verniers, J., Van Grootel, G., 1991. Review of the Silurian in the Brabant Massif, Belgium. Ann. Soc. Geol. Belg. 114, 163–193.

Verniers J., Herbosch, A., Vanguestaine, M., Geukens, F., Delcambre, B., Pingot, J., Belanger, I., Hennebert, M., Debacker, T., Sintubin, M., De Vos, W. Cambrian–Ordovician–Silurian lithostratigraphical units (Belgium). Geologica Belgica, in press.

Yurtsever, Y., Gat, J.R., 1981. Atmospheric waters. In: Gat, J.R., Gonfiantini, R. (Eds.), Stable Isotope Hydrology: Deuterium and Oxygen-18 in the Water Cycle. Int. Atomic Energy Agency, Vienna, Techn. Reports Series 210, 103–142.